Available online at www.sciencedirect.com
SCIENCE DIRECT
International Journal of Heat and Mass Transfer 49 (2006) 995–1003
International Journal of HEAT and MASS TRANSFER
www.elsevier.com/locate/ijhmt

# Time evolution of double-diffusive convection in a vertical cylinder with radial temperature and axial solutal gradients

Kefeng Shi, Wen-Qiang Lu *

*College of Physical Sciences, Graduate School of the Chinese Academy of Sciences, Beijing 100049, China*

Received 17 March 2005; received in revised form 20 September 2005
Available online 17 November 2005

**Abstract**

The characteristics of transient double-diffusive convection in a vertical cylinder are numerically simulated using a finite element method. Initially the fluid in the cavity is at uniform temperature and solute concentration, then constant temperature and solute concentration, which are lower than their initial values, are imposed along the sidewall and bottom wall, respectively. The time evolution of the double-diffusive convection is investigated for specific parameters, which are the Prandtl number, $Pr = 7$, the Lewis number, $Le = 5$, the thermal Grashof number, $Gr_T = 10^7$, and the aspect ratio, $A = 2$, of the enclosure. The objective of the work is to identify the effect of the buoyancy ratio (the ratio of solutal Grashof to thermal Grashof numbers: $N = Gr_S/Gr_T$) on the evolution of the flow field, temperature and solute field in the cavity. It is found that initially the fluid near the bottom wall is squeezed by the cold flow from the sidewall, a crest of the solute field forms and then pushed to the symmetry line. In the case of $N > 0$, a domain with higher temperature and weak flow (dead region) forms on the bottom wall near the symmetry line, and the area of dead region increases when $N$ varies from 0.5 to 1.5. More crests of the solute field are formed and the flow near the bottom wall fluctuates continuously for $N < 0$. The frequency of the fluctuation increases when $N$ varies from $-0.5$ to $-1.5$. Corresponding to the variety of the thermal and solutal boundary layers, the average rates of heat transfer ($Nu$) at the sidewall remain almost unchanged while the average rates of mass transfer ($Sh$) at the bottom wall change much in the cases of $N = 1, 0, -1$.


*Keywords:* Double-diffusive convection; Buoyancy ratio; Dead region; Fluctuation

## 1. Introduction

Double-diffusive convection is formed due to the combination of temperature and concentration gradients in the fluid, in which the thermal and mass diffusivities are different, and the heat and mass transfer occur simultaneously. Double-diffusive convection occurs in a wide range of scientific field such as biology, oceanography, astrophysics, geology, chemical processes and crystal-growth techniques [1–7]. Huppert and Turner [8] had presented an early review of the important developments in double-diffusive convection and the result of a close interaction between theoreticians, laboratory experimenters and sea-going oceanographers. In the past, most of the work done on the double-diffusive convection is focused on rectangular enclosures with aiding or opposing solutal gradient. Bejan [9] reported a fundamental study of a scale analysis relative to heat and mass transfer within a rectangular enclosure when the buoyancy effect is due to density variations caused by either temperature or solute concentration variations. Other studies within rectangular cavities were carried out by Murty [10], Lee and Hyun [11] and Sundaravadivelu and Kandaswamy [12].

As the rapid development of modern electronics industry, more interests in transport phenomena of crystal growth have been expanded. During the growth of a crystal, a good understanding of the buoyancy convection flows in this problem is necessary since it associates closely

* Corresponding author. Tel.: +86 10 88256277; fax: +86 10 62395850.
*E-mail address:* luwq@gscas.ac.cn (W.-Q. Lu).

0017-9310/$ - see front matter © 2005 Elsevier Ltd. All rights reserved.
doi:10.1016/j.ijheatmasstransfer.2005.09.009

**Nomenclature**

| | |
|---|---|
| $A$ | aspect ratio $A = H/R$ |
| $C$ | dimensionless solute concentration $(C^* - C_0^*)/(C_0^* - C_w^*)$ |
| $C^*$ | solute concentration |
| $D$ | mass diffusive coefficient ($m^2/s$) |
| $Gr_S$ | solutal Grashof number |
| $Gr_T$ | thermal Grashof number |
| $g$ | gravitational acceleration ($m/s^2$) |
| $H$ | height of the enclosure (m) |
| $Le$ | Lewis number |
| $N$ | buoyancy ratio $N = Gr_S/Gr_T$ |
| $Nu$ | average Nusselt number |
| $Pr$ | Prandtl number |
| $r$, $z$ | dimensionless radial and axial coordinates, $r = r^*/H$, $z = z^*/H$ |
| $r^*$, $z^*$ | radial and axial coordinate (m) |
| $R$ | radius of the enclosure (m) |
| $Sh$ | average Sherwood number |
| $t$ | dimensionless time |
| $T$ | dimensionless temperature $(T^* - T_0^*)/(T_0^* - T_w^*)$ |
| $T^*$ | temperature (K) |
| $u_r$, $u_z$ | dimensionless radial and axial velocity |
| $u_r^*$, $u_z^*$ | radial and axial velocity (m/s) |

*Greek symbols*

| | |
|---|---|
| $\alpha$ | thermal diffusive coefficient ($m^2/s$) |
| $\beta_S$ | coefficient of solutal expansion ($kg^{-1}$) |
| $\beta_T$ | coefficient of thermal expansion ($K^{-1}$) |
| $\nu$ | kinematic viscosity ($m^2/s$) |
| $\rho$ | density ($kg/m^3$) |
| $\psi$ | dimensionless stream-function |
| $\psi^*$ | stream-function |
| $\omega$ | dimensionless vorticity |
| $\omega^*$ | vorticity |

*Superscript*

| | |
|---|---|
| * | dimensional quantities |

*Subscripts*

| | |
|---|---|
| S | solutal |
| T | thermal |

to the local growth conditions and the overall transport rate. Chamkha and Al-Naser [13] indicated that the poor crystal quality is produced due to turbulence and predicted numerically the characteristics of hydromagnetic double-diffusive convective flow of a binary gas mixture in a rectangular enclosure with horizontal temperature and concentration gradients for $Pr = 1$, $Le = 2$ and $Ra_T = 10^5$. Chakraborty and Dutta [14] investigated the double-diffusive convection on account of solutal undercooling during non-equilibrium solidification of binary alloys. In addition, the related experimental studies dealing with the formation of the double-diffusive convection in the solidification of a binary mixture were carried out [15–17].

Recently, there has been a focus on transient processes in order to understand the oscillatory regime which occurs for a certain range of the Grashof number and the buoyancy ratio. Ghorayeb et al. [18] and Zhou and Zebib [19] numerically studied the unsteady double-diffusive convection in a horizontal container which is subjected to simultaneous horizontal temperature and concentration gradients to predict the critical $Gr_T$. Nishimura et al. [20] predicted that oscillatory double-diffusive convection occurs for a certain range of buoyancy ratio in a rectangular enclosure with combined horizontal temperature and concentration gradients. Bennacer et al. [21] investigated numerically and analytically the transient double-diffusive convection in a rectangular enclosure with horizontal temperature and vertical solutal gradients under the condition $Pr = 7$, $Le = 100$ and $A = 2.0$, the analysis was focused on a range of solutal to thermal buoyancy ratios ($0.5 \leqslant N \leqslant 10.0$). All these transient simulations are based only on the initial steady flow, and the gradients are formed by imposing different constant temperatures and solute concentration conditions on two vertical or horizontal walls. In addition, Sezai and Mohamad [22] pointed out that there is a possibility of symmetric breaking even though the boundary conditions are symmetric and reported that the flow in a cubic enclosure subject to horizontal and opposing gradients of heat and solute may become three dimensional which cannot be detected by 2-D models. As a first approximation, two-dimensional model is usually used to investigate the fundamental characters of the problem.

As far as authors' knowledge is concerned, the numerical studies of transient evolution of the double-diffusive convection in a vertical cylinder cavity have seldom been dealt with in literatures, especially imposed cross thermal and solutal gradients. However, the transient processes of double-diffusive convection in circular container have some special characters and it is of interest in both basic fluid dynamic and practical applications, such as the production of stratified fluid system and the Bridgman crystal-growth procedure in which the cross thermal and solutal gradients exist in the melt area. It should mention that Lin and Armfield [23] directly simulated the natural convection cooling in a vertical cylinder, which is driven by thermal buoyancy alone. Moreover, Mohamad and Bennacer [24,25] investigated numerically the double-diffusive convection in a rectangular enclosure filled with saturated porous medium which is submitted to the cross gradients of heat and solute. Sung et al. [26] numerically studied double-diffusive convection in a rotating annulus with horizontal thermal

gradient and vertical solutal gradient for $Pr = 1.0$, $Le = 10.0$, $Ra_T = 10^5$ and $N > 0$.

In this paper, we restrict ourselves to the investigation of the structure of time-dependent double-diffusive convection in a vertical cylinder. In the following, a vertical cylinder with radial temperature and axial concentration gradients is considered. The transient evolution characters of the double-diffusive convection from the initial rest fluid, for different buoyancy ratio ($N > 0$ and $N < 0$), are investigated in detail and compared with the convection driven only by a thermal buoyancy ($N = 0$). The work focuses on the effects of the buoyancy ratio on the characters of the flow, heat and mass transfer rates. Some significant new results are obtained for the range of the buoyancy ratio (from $-1.5$ to 1.5).

## 2. Numerical method

### 2.1. Mathematical model

The physical system is a vertical cylinder with a height of $H$ and a radius of $R$, and the aspect ratio $A = H/R$ (see Fig. 1). The following assumptions are made. The binary fluid is Newtonian and the flow in the cylinder is axisymmetric, incompressible and laminar. The heat generation, viscous dissipation, chemical reactions and thermal radiation are neglected. The Boussinesq approximation is used. In the buoyancy term, the fluid density is expressed as $\rho(T^*, C^*) = \rho_0(1 - \beta_T(T^* - T_0^*) - \beta_S(C^* - C_0^*))$, where, $\rho_0 = \rho(T_0^*, C_0^*)$, $\beta_T = (-1/\rho_0)\ (\partial\rho/\partial T^*)_{C^*}$ and $\beta_S = (-1/\rho_0)\ (\partial\rho/\partial C^*)_{T^*}$ are the density at temperature $T_0^*$ and solute concentration $C_0^*$, the thermal expansion coefficient and the solutal expansion coefficient, respectively. The governing equations are written by employing a vorticity-stream function formulation. The stream function $\psi^*$ and vorticity $\omega^*$ are defined in terms of the radial velocity $(u_r^*)$ and axial velocity $(u_z^*)$ as

$$u_r^* = \frac{1}{r^*}\frac{\partial\psi^*}{\partial z^*}, \quad u_z^* = -\frac{1}{r^*}\frac{\partial\psi^*}{\partial r^*} \tag{1}$$

$$\omega^* = \frac{\partial u_r^*}{\partial z^*} - \frac{\partial u_z^*}{\partial r^*} \tag{2}$$

On the basis of the above assumption, the conservation equations for vorticity, stream-function, energy and species in dimensionless form are written as follows.

*Vorticity equation:*

$$\frac{\partial\omega}{\partial t} + \frac{1}{r}\frac{\partial\psi}{\partial z}\frac{\partial\omega}{\partial r} - \frac{1}{r}\frac{\partial\psi}{\partial r}\frac{\partial\omega}{\partial z} - \frac{\omega}{r^2}\frac{\partial\psi}{\partial z} = \left(\frac{\partial^2\omega}{\partial r^2} + \frac{1}{r}\frac{\partial\omega}{\partial r} + \frac{\partial^2\omega}{\partial z^2} - \frac{\omega}{r^2}\right) - Gr_T\left(\frac{\partial T}{\partial r} + N\frac{\partial C}{\partial r}\right) \tag{3}$$

*Stream-function equation:*

$$\frac{\partial^2\psi}{\partial r^2} + \frac{\partial^2\psi}{\partial z^2} - \frac{1}{r}\frac{\partial\psi}{\partial r} = r\omega \tag{4}$$

*Energy equation:*

$$\frac{\partial T}{\partial t} + \frac{1}{r}\frac{\partial\psi}{\partial z}\frac{\partial T}{\partial r} - \frac{1}{r}\frac{\partial\psi}{\partial r}\frac{\partial T}{\partial z} = \frac{1}{Pr}\left(\frac{\partial^2 T}{\partial r^2} + \frac{1}{r}\frac{\partial T}{\partial r} + \frac{\partial^2 T}{\partial z^2}\right) \tag{5}$$

*Species equation:*

$$\frac{\partial C}{\partial t} + \frac{1}{r}\frac{\partial\psi}{\partial z}\frac{\partial C}{\partial r} - \frac{1}{r}\frac{\partial\psi}{\partial r}\frac{\partial C}{\partial z} = \frac{1}{PrLe}\left(\frac{\partial^2 C}{\partial r^2} + \frac{1}{r}\frac{\partial C}{\partial r} + \frac{\partial^2 C}{\partial z^2}\right) \tag{6}$$

where $Gr_T = \frac{g\beta_T\Delta T^* H^3}{\nu^2}$, $Gr_S = \frac{g\beta_S\Delta C^* H^3}{\nu^2}$, $Pr = \frac{\nu}{\alpha}$, $Le = \frac{\alpha}{D}$ and $N = \frac{Gr_S}{Gr_T}$. In the above equations, lengths are non-dimensionalized by $H$, stream-function by $H\nu$, vorticity by $\nu/H^2$, time by $H^2/\nu$, $(T^* - T_0^*)$ by $\Delta T^*$ $(\Delta T^* = T_0^* - T_w^*)$ and $(C^* - C_0^*)$ by $\Delta C^*$ $(\Delta C^* = C_0^* - C_w^*)$.

Initially the fluid in the cylinder is at rest, at uniform temperature $(T = 0)$ and solute concentration $(C = 0)$. At $t = 0$ the temperature on the sidewall changes impulsively to $T = -1$ and the solute concentration on the bottom wall varies to $C = -1$, this temperature and solute concentration are kept constant thereafter. The corresponding initial and boundary conditions in dimensionless form can be written as follows:

$$\psi = \omega = 0, \quad T = C = 0 \text{ at all } (r, z) \text{ and } t < 0 \tag{7}$$

$$\psi = 0, \quad \frac{\partial T}{\partial r} = \frac{\partial C}{\partial r} = 0 \text{ on } r = 0 \text{ for } t \geqslant 0 \tag{8}$$

$$\psi = 0, \quad \frac{\partial C}{\partial z} = 0, \quad T = -1 \text{ on } r = 1/A \text{ for } t \geqslant 0 \tag{9}$$

$$\psi = 0, \quad \frac{\partial T}{\partial z} = 0, \quad C = -1 \text{ on } z = 0 \text{ for } t \geqslant 0 \tag{10}$$

$$\psi = 0, \quad \frac{\partial T}{\partial z} = \frac{\partial C}{\partial z} = 0 \text{ on } z = 1 \text{ for } t \geqslant 0 \tag{11}$$

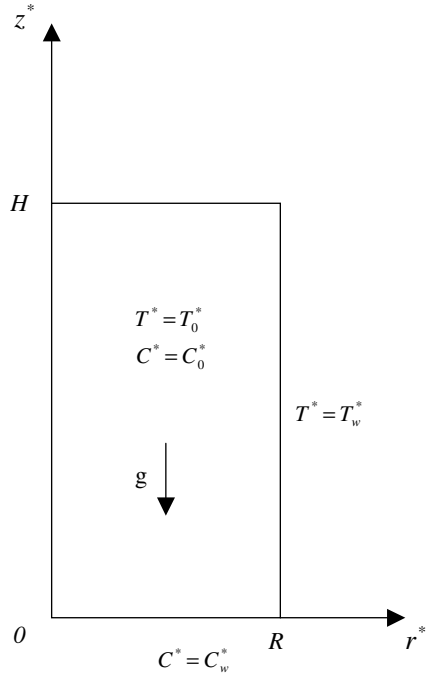


Fig. 1. Computational domain and coordinate system.

The dimensionless average rates of heat transfer across the side wall and mass transfer across the bottom wall are expressed by the Nusselt and Sherwood numbers, respectively:

$$Nu = \int_0^1 \left(\frac{\partial T}{\partial r}\right)_{r=1/A} \mathrm{d}z \tag{12}$$

$$Sh = \int_0^{1/A} \left(\frac{\partial C}{\partial z}\right)_{z=0} \mathrm{d}r \tag{13}$$

### 2.2. Numerical scheme

The control equations are solved numerically by a finite element method and the temperature and solute concentration fields then can be simulated. Rectangular elements with four nodes are used, in which bilinear function is constructed: $\Phi = b_1 + b_2\xi + b_3\eta + b_4\xi\eta$.

The numerical method has been employed by authors [27,28] to study the steady double-diffusive convection in vertical rectangular and annular cavities with horizontal temperature and solutal gradients and cross temperature and solutal gradients, respectively. Some reasonable results have been obtained, and the results in rectangular cavity [27] agree well with Ghorayeb et al. [18]. In order to investigate the transient problem, implicit Euler backward scheme is used to discretize the time derivative terms. The variable band matrix equations are solved using Gauss elimination method. The solution of the equations is carried out in the following way. First step, all variables are known at $t = n\Delta t$. Second step, Eqs. (5) and (6) are solved to obtain the initial approximation to $T^{n+1}$ and $C^{n+1}$, and the derivatives of temperature and concentration are calculated. Third step, using the values of second step, Eqs. (3) and (4) are solved to obtain a first approximation to $\omega^{n+1}$ and $\psi^{n+1}$. Final step, if the values of vorticity at the boundary wall satisfy $\left|\frac{\omega^{n+1}-\omega^n}{\omega^n}\right| \leqslant \varepsilon = 10^{-5}$, then time is progressed and this procedure is repeated; otherwise, relaxation iteration is used to get new estimate of $\omega^n$ at the boundary wall and return back the first step, the procedure is repeated until the convergence accuracy is achieved, then time is progressed.

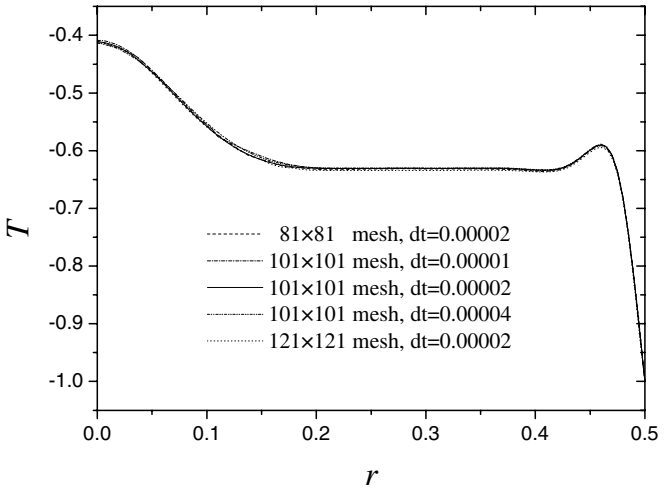


Fig. 2. Comparison of the results for different mesh schemes: the radial profiles of temperature at mid-height $z = 0.5$ and $t = 0.025$.

To test the grid independence of the scheme, the solutions have been obtained on the meshes of $81 \times 81$, $101 \times 101$ and $121 \times 121$, respectively. In addition, different time steps ($\mathrm{d}t = 0.00001$, $\mathrm{d}t = 0.00002$ and $\mathrm{d}t = 0.00004$) for mesh $101 \times 101$ are chosen. The profiles of temperature as a function of radial distance at mid-height for $t = 0.025$ are shown in Fig. 2. The differences between the results of different mesh schemes are very small, so the mesh $101 \times 101$ ($\mathrm{d}t = 0.00002$) is chosen in the present computation.

## 3. Results and discussion

The controlling parameters of the fluid flow and heat and mass transfer rates for the double-diffusive convection in an enclosure are thermal Grashof number, $Gr_T$, Prandtl number, $Pr$, buoyancy ratio, $N = Gr_S/Gr_T$, Lewis number, $Le$, and aspect ratio, $A$. In this paper, the parameters are chosen as: $Gr_T = 10^7$, $Pr = 7$, $Le = 5$ and $A = 2$. In the following numerical examples, the coefficient of thermal expansion $\beta_T$ is assumed to positive which means that the fluid density $\rho$ decreases with increasing $T$. In the case of $N > 0$, it leads to a solute Grashof number $Gr_S > 0$ and the coefficient of solutal expansion $\beta_S > 0$; this means that $\rho$ increases with decreasing $C$. For $N < 0$, the case is opposite, i.e. $Gr_S < 0$, $\beta_S < 0$, it means $\rho$ decreases with decreasing $C$.

### 3.1. The evolution of thermal field and solutal field

Fig. 3 displays the thermal driven convection course for $N = 0$. In Fig. 3(a), it is seen that a vertical thermal boundary layer develops very rapidly on the sidewall. After the full development of the vertical thermal boundary layer, a cold flow begins to form and moves continuously along the bottom wall towards the symmetry line. As the intrusion approaches the symmetry line, it extends along the symmetry line first and then falls down to form a complicated flow in the lower part of the cavity. As the fluid in the lower part of the cavity loses its momentum gradually and with the diffusion of thermal, the temperature stratification generates in the cavity ultimately. These phenomena compare well with the results reported by Lin and Armfield [23]. From the picture of solutal field shown in Fig. 3(b), it is observed that a crest of solutal field forms and pushed to the symmetry line because the fluid of solutal boundary layer along the bottom wall is squeezed by the cold flow. After the crest reaches the symmetry line, it travels up along the symmetry line.

Figs. 4 and 5 illustrate the double-diffusive convection in the cases of $N = 1$ and $-1$. There are some interesting characters, which are different from Fig. 3, because of the presence of solutal buoyancy. In the case of $N = 1$,

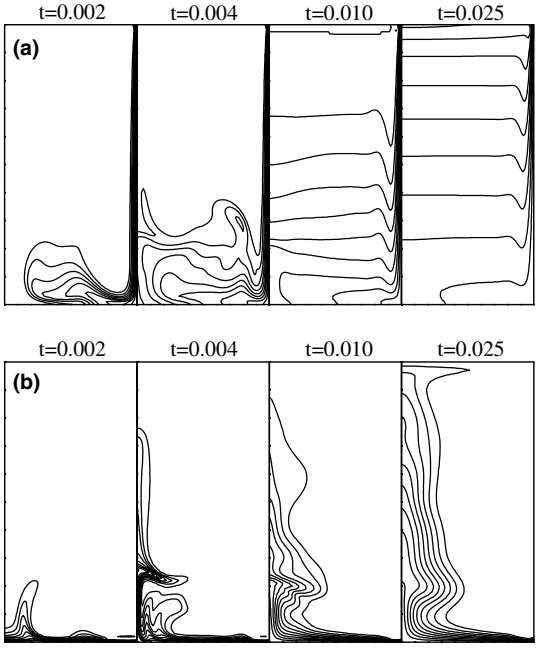


Fig. 3. Time evolution of the transient thermal field (a) and solutal field (b) for the thermal convection of $N = 0$ in the cavity.

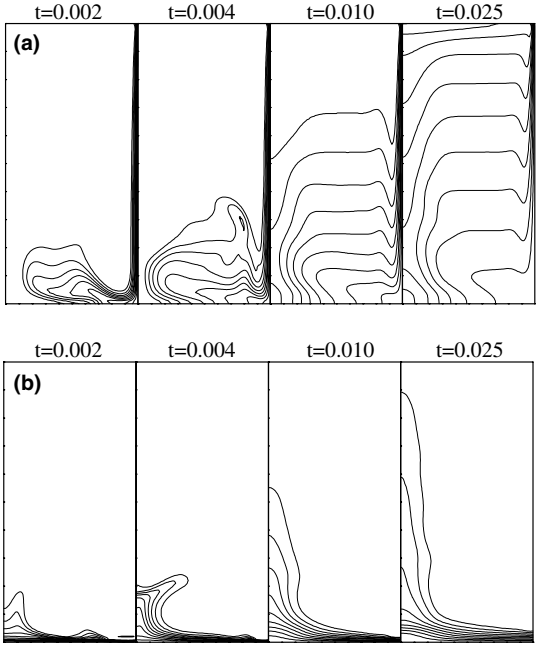


Fig. 4. Time evolution of the transient thermal field (a) and solutal field (b) for the double-diffusive convection of $N = 1$ in the cavity.

as mentioned above, the density of the fluid in the solutal boundary layer near the bottom wall increases. Hence, as shown in Fig. 4, the cold flow near the bottom wall is restrained and the rate of the development of solutal field along the symmetry line slows down in contrast to the case of $N = 0$. Finally, a domain in which the temperature remains relatively high appears near the bottom of the

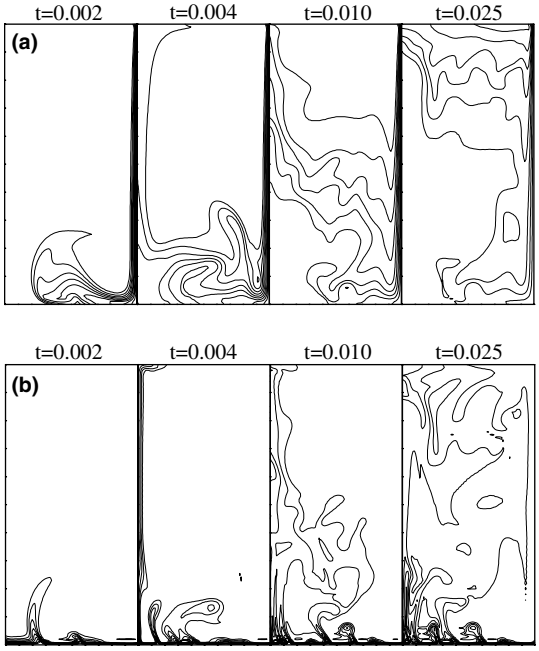


Fig. 5. Time evolution of the transient thermal field (a) and solutal field (b) for the double-diffusive convection of $N = -1$ in the cavity.

symmetry line, which is called a dead region. On the contrary, in the case of $N = -1$, after being squeezed by the cold flow, the fluid near the bottom wall moves upward easily because of its low density, as shown in Fig. 5; as a result, more crests of the solutal field are formed and the flow in the cavity becomes chaotic during the evolution due to the opposite direction of thermal and solutal buoyancy.

### 3.2. Transient flow features

In order to provide a comprehensive and direct perception of the flow structure in the cavity, Figs. 6 and 7 summarize the time traces of the velocity at two specific points

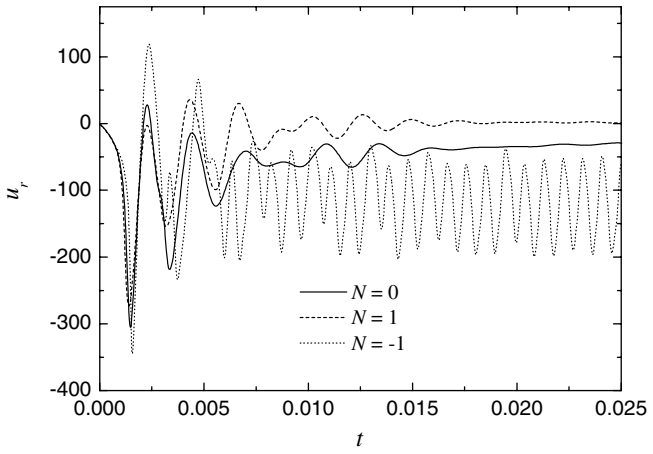


Fig. 6. Time traces of radial velocity at location $r = 0.25$ and $z = 0.02$.

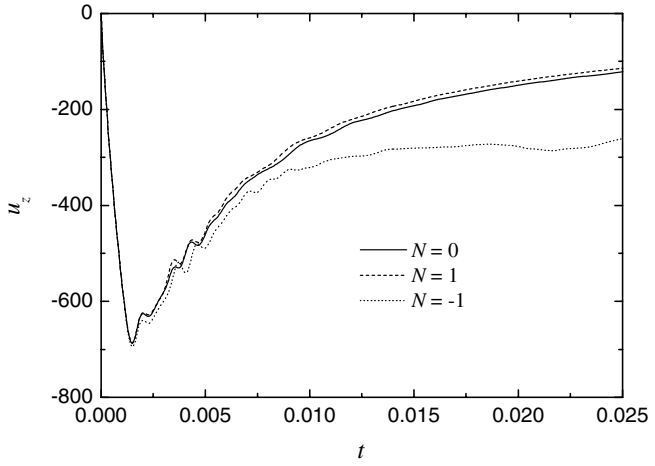


Fig. 7. Time traces of vertical velocity at location $r = 0.49$ and $z = 0.25$.

($r = 0.25$, $z = 0.02$ and $r = 0.49$, $z = 0.25$), which are near the bottom wall and side wall, respectively. In Fig. 6, it is clear that the flow structures near the bottom wall are different in the case of $N = 1, 0, -1$. Fig. 6 illustrates that the magnitudes of radial velocity in the case of $N = 1$ are smaller than that of $N = 0$ since cold flow is restrained by the heavier fluid near the bottom wall. In the case of $N = -1$, as mentioned above, the density of the fluid in the solutal boundary layer near the bottom wall will be light and the flow is enhanced (Fig. 6). In addition, the flow is affected due to the formation of the crests of solute field near the bottom wall, so the traces of radial velocity fluctuate all the time. In Fig. 7, it is observed that the flow structures near the sidewall, for the cases of $N = 0$ and 1, are similar, but the trace for $N = -1$ separates from them obviously in the latter course and there are no fluctuations.

### 3.3. Dead region for $N > 0$

As shown in Fig. 4, in the case of $N > 0$, a dead region with weak flow and heat transfer is formed near the bottom of the symmetry line. For $N > 0$, when the solute concentration at the bottom wall remains constant $C = -1$, the density of the fluid near the bottom wall will increase due to $\beta_S > 0$. When the fluid in the solutal boundary near the bottom wall is pushed to the symmetry line, it will be difficult to move upward because its density increases, where the heavy fluid is gathered. As a result, the flow turns upward before it approaches the symmetry line and then a dead region appears, as shown in Fig. 8(a). On the contrary, Fig. 8(b) indicates that the flow is much stronger at the bottom of symmetry line in the case of $N = 0$. At the same time, Fig. 9 displays thermal field near the bottom of the symmetry line for $N = 0$, 0.5, 1.0 and 1.5 at $t = 0.02$. It is observed that the dead region will form gradually and its area will increase as $N$ changes from 0 to 1.5.

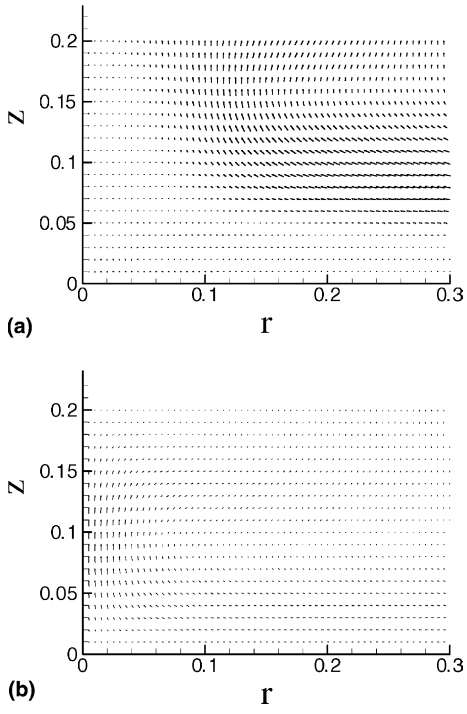


Fig. 8. Velocity vector graph for $N = 1$ (a) and $N = 0$ (b) at $t = 0.02$.

### 3.4. Fluctuation near the bottom wall for $N < 0$

For $N < 0$, the density of the fluid in the solutal boundary layer near the bottom wall will decrease in the current case ($C = -1$ at $z = 0$). As shown in Fig. 5, the fluid near the bottom wall is squeezed by the cold flow, and then the crests of solutal field form continuously due to the upward buoyancy force. These discontinuous upward flows (crests) induce the oscillation of the traces. Fig. 10 depicts the fluctuant traces of radial velocity near the bottom wall. It is clear that the fluctuations of the traces are different according the $N$ values. When the buoyancy ratio $N$ changes from $-0.5$ to $-1.5$, the frequency of the oscillation increases.

### 3.5. Nu and Sh

The average Nusselt number, $Nu$, at the sidewall and the average Sherwood number, $Sh$, at the bottom wall are depicted in Fig. 11 for different $N$. It is observed that $Nu$ changes little as the buoyancy ratio $N$ varies; however, the variations of $Sh$ for different buoyancy ratio $N$ are obvious. These results are associated with the different patterns of the thermal and solutal boundary layers. The variations of the boundary layer lead to the change of the thermal and solutal gradients, which result in the variation of $Nu$ and $Sh$. As shown in Figs. 3–5, the solutal boundary layers near the bottom wall are different from each other for different $N$, and the vibration of the boundary layer leads to the fluctuation of $Sh$ for $N = -1$. However, the thermal boundary layers near the sidewall are almost sim-

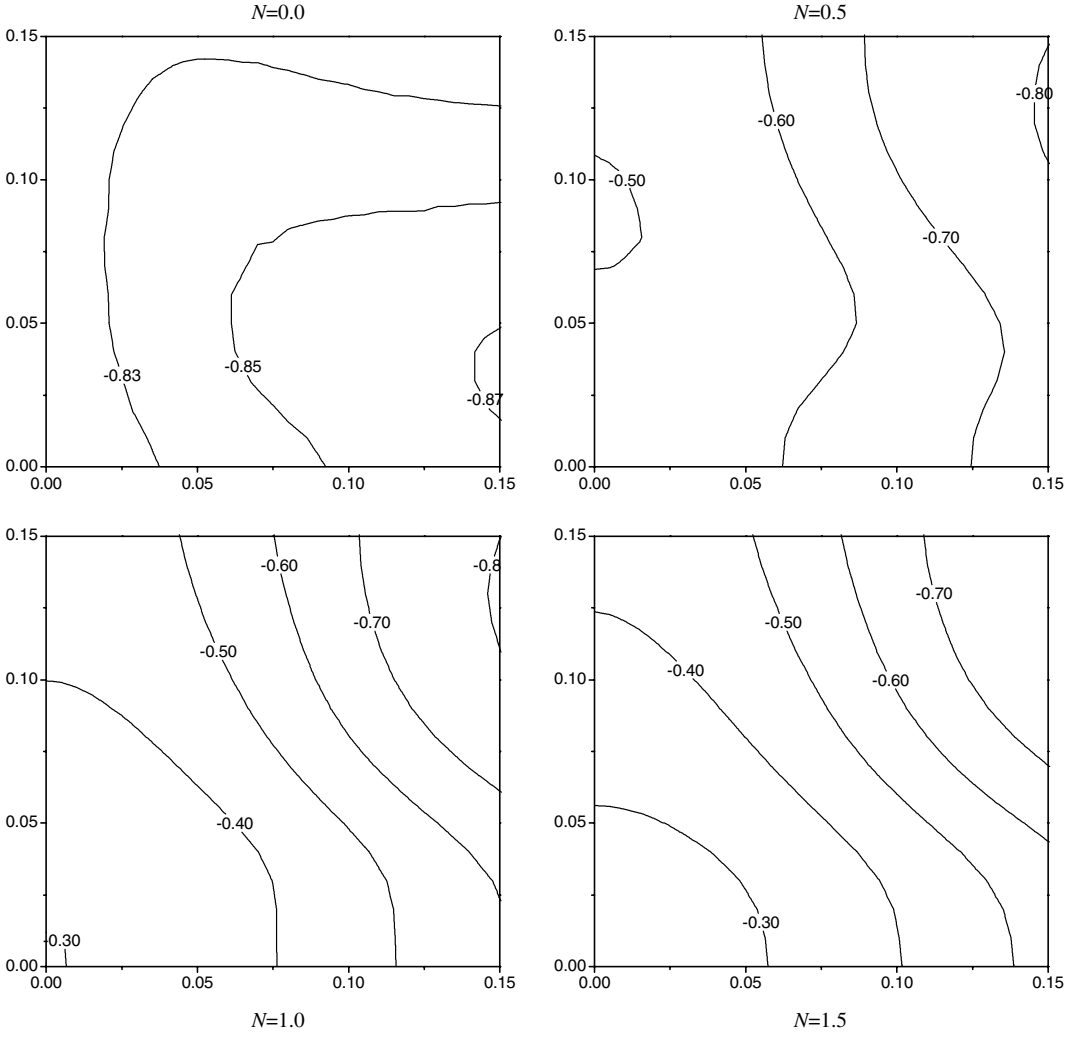


Fig. 9. The formation and variation of dead region at $t = 0.02$.

ilar for $N = 1$, 0 and $-1$, which leads that the variations of $Nu$ are very small (Fig. 11(a)).

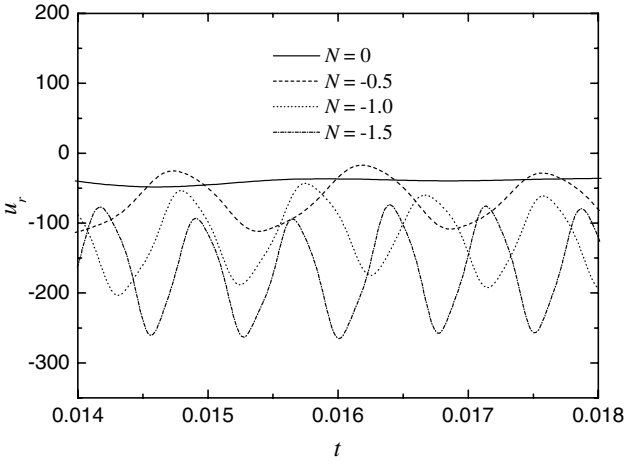


Fig. 10. Time traces of radial velocity at point $r = 0.25$ and $z = 0.02$.

## 4. Conclusions

Numerical solutions are obtained for the transient process of the double-diffusive convection in a vertical cylinder with radial temperature and axial solutal gradients. The presented results exhibit a comprehensive and direct perception of the transient evolving process of the double-diffusive convection from the initial rest fluid, at the same time, new features of the double-diffusive convection are observed for a given range of buoyancy ratio. The following conclusive remarks have been drawn:

(1) Due to the cold flow from the sidewall, the fluid near the bottom wall is squeezed, a crest of solutal field forms and then will be pushed to the symmetry line. After the crest reaches the symmetry line, it travels up along the symmetry line.
(2) In the case of $N > 0$, the flow near the bottom wall is restrained and a dead region forms. The area of the dead region increases with increasing $N$ from 0 to

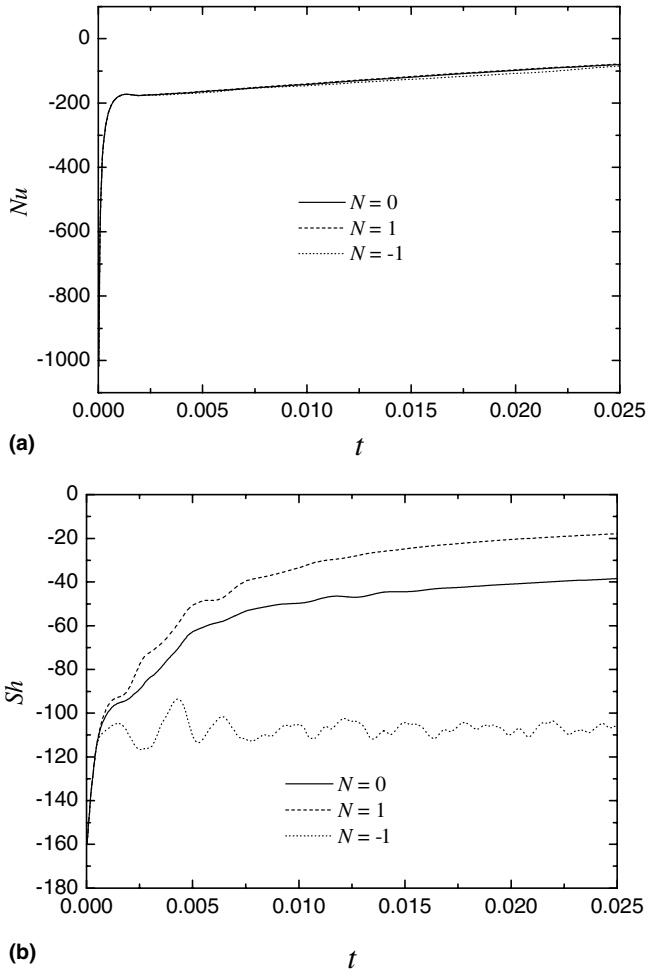


Fig. 11. The average *Nu* (a) at the sidewall and the average *Sh* (b) at the bottom wall.

1.5 and the temperature at that region also increases with the increasing $N$.

(3) For $N < 0$, more crests of the solutal field are formed and the flow fluctuates continuously near the bottom wall due to the opposite directions of thermal and solutal buoyancy. The frequency of the fluctuation depends on the magnitude of $N$. When $N$ changes from $-0.5$ to $-1.5$, the frequency of the fluctuation increases.

(4) Under the conditions of $N = 1$, 0 and $-1$, the Nusselt number at the sidewall changes little while the Sherwood number at the bottom wall varies considerably. This is consistent with the different patterns of the thermal boundary layers on the sidewall and the solutal boundary layers on the bottom wall for different $N$.

## Acknowledgement

This work is supported by the National Natural Science Foundation of China (Grant no. 50336040).

## References

[1] B. Rudels, G. Björk, R.D. Muench, U. Schauer, Double-diffusive layering in the Eurasian Basin of the Arctic Ocean, J. Mar. Syst. 21 (1–4) (1999) 3–27.

[2] E. Özsoy, Ü. Ünlüata, Z. Top, The evolution of Mediterranean water in the Black Sea: interior mixing and material transport by double-diffusive intrusions, Prog. Oceanogr. 31 (3) (1993) 275–320.

[3] R.O. Fournier, Double-diffusive convection in geothermal systems: the Salton Sea, California, geothermal system as a likely candidate, Geothermics 19 (6) (1990) 481–496.

[4] M. Marcoux, M.C. Charrier-Mojtabi, M. Azaiez, Double-diffusive convection in an annular vertical porous layer, Int. J. Heat Mass Transfer 42 (13) (1999) 2313–2325.

[5] M. Markus, Double-diffusive convection: a simple demonstration, J. Chem. Educ. 81 (4) (2004) 526–529.

[6] M. Mamou, Stability analysis of the perturbed rest state and of the finite amplitude steady double-diffusive convection in a shallow porous enclosure, Int. J. Heat Mass Transfer 46 (12) (2003) 2263–2277.

[7] W. Lan, C.Y. Tu, Morphological instability due to double-diffusive convection in directional solidification: the pit formation, J. Cryst. Growth 220 (4) (2000) 619–630.

[8] H.E. Huppert, J.S. Turner, Double-diffusive convection, J. Fluid Mech. 106 (1981) 299–329.

[9] A. Bejan, Mass and heat transfer by nature convection in a vertical cavity, Int. J. Heat Fluid Flow 6 (3) (1985) 149–159.

[10] V.D. Murty, A finite element solution of double-diffusive convection, Int. Commun. Heat Mass Transfer 15 (2) (1988) 165–177.

[11] J.W. Lee, J.M. Hyun, Time-dependent double diffusion in a stably stratified fluid under lateral heating, Int. J. Heat Mass Transfer 34 (9) (1991) 2409–2421.

[12] K. Sundaravadivelu, P. Kandaswamy, Double diffusive nonlinear convection in a square cavity, Fluid Dyn. Res. 27 (5) (2000) 291–303.

[13] A.J. Chamkha, H. Al-Naser, Hydromagnetic double-diffusive convection in a rectangular enclosure with opposing temperature and concentration gradients, Int. J. Heat Mass Transfer 45 (12) (2002) 2465–2483.

[14] S. Chakraborty, P. Dutta, The effect of solutal undercooling on double-diffusive convection and macrosegregation during binary alloy solidification: a numerical investigation, Int. J. Numer. Meth. Fluids 38 (9) (2002) 895–917.

[15] F.L. Chen, Formation of double-diffusive layers in the directional solidification of binary solution, J. Cryst. Growth 179 (1–2) (1997) 277–286.

[16] C. Ghenai, A. Mudunuri, C.X. Lin, et al., Double-diffusive convection during solidification of a metal analog system ($NH_4Cl$–$H_2O$) in a differentially heated cavity, Exp. Therm. Fluid Sci. 28 (1) (2003) 23–35.

[17] T. Nishimura, T. Imoto, Occurrence and development of double-diffusive convection during solidification of a binary system, Int. J. Heat Mass Transfer 37 (10) (1994) 1455–1464.

[18] K. Ghorayeb, H. Khallouf, A. Mojtabi, Onset of oscillatory flows in double-diffusive convection, Int. J. Heat Mass Transfer 42 (4) (1999) 629–643.

[19] H. Zhou, A. Zebib, Oscillatory double-diffusive convection in crystal growth, J. Cryst. Growth 135 (3–4) (1994) 587–593.

[20] T. Nishimura, M. Wakamatsu, A.M. Morega, Oscillatory double-diffusive convection in a rectangular enclosure with combined horizontal temperature and concentration gradients, Int. J. Heat Mass Transfer 41 (11) (1998) 1601–1611.

[21] R. Bennacer, A.A. Mohamad, D. Akrour, Transient natural convection in an enclosure with horizontal temperature and vertical solutal gradients, Int. J. Therm. Sci. 40 (10) (2001) 899–910.

[22] I. Sezai, A.A. Mohamad, Double diffusive convection in a cubic enclosure with opposing temperature and concentration gradients, Phys. Fluids 12 (9) (2000) 2210–2223.

[23] W.X. Lin, S.W. Armfield, Direct simulation of natural convection cooling in a vertical circular cylinder, Int. J. Heat Mass Transfer 42 (22) (1999) 4117–4130.

[24] A.A. Mohamad, R. Bennacer, Natural convection in a confined saturated porous medium with horizontal temperature and vertical solutal gradients, Int. J. Therm. Sci. 40 (1) (2001) 82–93.

[25] A.A. Mohamad, R. Bennacer, Double diffusion, natural convection in an enclosure filled with saturated porous medium subjected to cross gradients; stably stratified fluid, Int. J. Heat Mass Transfer 45 (18) (2002) 3725–3740.

[26] H.J. Sung, W.K. Cho, J.M. Hyun, Double-diffusive convection in a rotating annulus with horizontal temperature and vertical solutal gradients, Int. J. Heat Mass Transfer 36 (15) (1993) 3773–3782.

[27] K.F. Shi, W.Q. Lu, Double-diffusive convection in an annular vertical cavity, J. Grad. School Chinese Acad. Sci. 22 (2) (2005) 152–156.

[28] K.F. Shi, W.Q. Lu, Numerical simulation of double-diffusive convection with cross gradients, J. Eng. Thermophys. 26 (2) (2005) 328–330.